Aryl hydrocarbon receptor deficiency causes dysregulated cellular matrix metabolism and age-related macular degeneration-like pathology

Peng Hu[a,1], Rolf Herrmann[a,1,2], Amanda Bednar[a], Peter Saloupis[a], Mary A. Dwyer[b], Ping Yang[a], Xiaoping Qi[c], Russell S. Thomas[d], Glenn J. Jaffe[a], Michael E. Boulton[c], Donald P. McDonnell[b], and Goldis Malek[a,e,3]

Departments of [a]Ophthalmology, [e]Pathology, and [b]Pharmacology and Cancer Biology, Duke University, Durham, NC 27710; [c]Department of Anatomy and Cell Biology, University of Florida, Gainesville, FL 32610; and [d]The Hamner Institutes for Health Sciences, Durham, NC 27709

Edited by Lincoln V. Johnson, University of California, Santa Barbara, CA, and accepted by the Editorial Board September 12, 2013 (received for review April 25, 2013)

The aryl hydrocarbon receptor (AhR) is a nuclear receptor that regulates xenobiotic metabolism and detoxification. Herein, we report a previously undescribed role for the AhR signaling pathway as an essential defense mechanism in the pathogenesis of early dry age-related macular degeneration (AMD), the leading cause of vision loss in the elderly. We found that AhR activity and protein levels in human retinal pigment epithelial (RPE) cells, cells vulnerable in AMD, decrease with age. This finding is significant given that age is the most established risk factor for development of AMD. Moreover, *AhR*$^{-/-}$ mice exhibit decreased visual function and develop dry AMD-like pathology, including disrupted RPE cell tight junctions, accumulation of RPE cell lipofuscin, basal laminar and linear-like deposit material, Bruch's membrane thickening, and progressive RPE and choroidal atrophy. High-serum low-density lipoprotein levels were also observed in *AhR*$^{-/-}$ mice. In its oxidized form, this lipoprotein can stimulate increased secretion of extracellular matrix molecules commonly found in deposits from RPE cells, in an AhR-dependent manner. This study demonstrates the importance of cellular clearance via the AhR signaling pathway in dry AMD pathogenesis, implicating AhR as a potential target, and the mouse model as a useful platform for validating future therapies.

retinal pigment epithelium | retinal disease | toxin metabolism | oxidized low density lipoprotein

Age-related macular degeneration (AMD) is the leading cause of vision loss in individuals over the age of 55 y in the Western world (1). It is a complex and heterogeneous disease, multifactorial with genetic, systemic health, and environmental factors regulating its initiation and progression (2, 3). Phenotypically, eyes with the dry clinical subtype are characterized by accumulation of focal and diffuse extracellular lipid protein-rich deposits below the retinal pigment epithelial cells (sub-RPE in 85–87% of cases) and/or within Bruch's membrane. These deposits include drusen, basal laminar, and basal linear deposits (4, 5) and are associated with RPE dysfunction, apoptosis, and ultimately degeneration. The latter of which, RPE atrophy and degeneration, is seen in an advanced form of dry AMD called geographic atrophy. Currently, there are no treatment options available for these patients. Despite advances in our understanding of the composition of sub-RPE deposits (6–8), the critical molecular events and signaling pathways leading to progressive RPE dysfunction and extracellular deposit biogenesis are still unknown.

One function crucial to cellular health is the cells ability to degrade harmful substances from exogenous and endogenous sources, ultimately preventing cellular accumulation of detrimental lipids and proteins. The aryl hydrocarbon receptor (AhR) signaling pathway is a major defense mechanism that has evolved to protect against toxin overload in cells under continual threat from metabolic waste products and xenobiotics. In that capacity, it regulates multiple phase I and II metabolic enzymes that metabolize endogenous and xenobiotic compounds, clearing cellular molecular garbage, thereby preventing further damage and aging (9). The AhR is a ligand-dependent transcription factor and a member of the Per-Arnt-Sim (PAS) superfamily of proteins. Although originally identified as the receptor for environmental contaminants such as polycyclic and halogenated aromatic hydrocarbons (PAH and HAH), constituents of cigarette smoke, byproducts of industrial combustion, automobile exhaust, and the human diet (10), mounting evidence indicates that this receptor has a number of diverse endogenous and exogenous ligands (11–13).

Studies on the mechanisms of AhR have mainly used the HAH 2,3,7,8-tetrachlorodibenzo-*p*-dioxin (TCDD) as the prototype ligand, which is resistant to environmental and biological degradation (14). Upon ligand binding, the PAS domain of the AhR heterodimerizes with a structurally related protein called the AhR nuclear translocator (ARNT). This complex then facilitates expression of a battery of genes encoding xenobiotic and drug-metabolizing enzymes [e.g., cytochrome P450 (*CYP*) 1A1, B1] and genes involved in extracellular matrix metabolism, cholesterol biosynthesis, ubiquitination and proteasomal degradation, and clearance (15–19).

Significance

Age-related Macular Degeneration (AMD) is the leading cause of vision loss. In its early stage, extracellular deposits accumulate below the retinal pigment epithelial layer (RPE), nurse cells to the retina. Identification of therapeutic treatments targeting deposit removal, which when left untreated exacerbate RPE and retinal damage, necessitates the discovery of pathways regulating deposit formation. We show that the activity of a nuclear receptor, essential to xenobiotic/toxin metabolism and cellular debris clearance, is critical to maintaining RPE cell health and that its deficiency in mice causes AMD pathology. This model provides a better understanding of AMD pathogenic mechanisms and a platform for testing novel therapeutics.

Author contributions: P.H., R.H., M.E.B., and G.M. designed research; P.H., R.H., A.B., P.S., M.A.D., X.Q., M.E.B., and G.M. performed research; P.Y., R.S.T., G.J.J., and D.P.M. contributed new reagents/analytic tools; X.Q., M.E.B., D.P.M., and G.M. analyzed data; and G.M. wrote the paper.

The authors declare no conflict of interest.

This article is a PNAS Direct Submission. L.V.J. is a guest editor invited by the Editorial Board.

Freely available online through the PNAS open access option.

[1]P.H. and R.H. contributed equally to this work.

[2]Present address: Departments of Ophthalmology and Cell Biology, Medical College of Wisconsin, Milwaukee, WI.

[3]To whom correspondence should be addressed. E-mail: gmalek@duke.edu.

This article contains supporting information online at www.pnas.org/lookup/suppl/doi:10.1073/pnas.1307574110/-/DCSupplemental.

Recent findings based on haplotype analysis of AMD versus control cases suggest that AhR may play a role in AMD susceptibility (20). This possible minor genetic association, along with the overlap between molecular events regulated by AhR, such as extracellular matrix proteolysis, cellular degradation and clearance, and events important in sub-RPE deposit formation, led us to hypothesize that the AhR signaling pathway may be important in AMD pathogenesis. To test this hypothesis, we determined the expression and activity of AhR as a function of age, given that age is the most established risk factor for development of AMD. We demonstrated that the AhR signaling pathway is active in RPE cells derived from human donor eye tissue. We examined visual function and morphology of eyes from mice harboring the null allele at the aryl hydrocarbon locus ($AhR^{-/-}$). We found that the AhR along with constituents of it canonical signaling pathway are present in human RPE cells, that AhR activity and protein levels in human RPE cells decrease with age, and that aged $AhR^{-/-}$ mice exhibit hallmark characteristics of dry AMD. Furthermore, we demonstrate that secretion of collagen IV, a known component of sub-RPE deposits, is seen from RPE cells following AhR knockdown and exacerbated following treatment with oxidized low-density lipoprotein (oxLDL). In vivo, in the absence of a functional AhR, serum LDL increases and consequently may stimulate further extracellular matrix production by RPE cells, supporting the hypothesis that decreased AhR activity promotes sub-RPE deposit formation, in part, through the effects of increased oxLDL on RPE cells.

Results

The AhR Signaling Pathway Is Active in Human RPE Cells. AhR activity can be investigated by (*i*) examining transcriptional activity, i.e., the binding of the receptor-ligand complex to the gene response element, and (*ii*) evaluating the expression of known AhR target genes. To determine whether the AhR signaling pathway is present in human RPE cells, we examined AhR and ARNT expression in ARPE19 cells, primary RPE (1-RPE) cell cultures, and freshly isolated human RPE cells (Fig. 1 *A* and *B*). We also assessed AhR transcriptional activity and target-gene expression in ARPE19 cells following treatment with known AhR agonists and antagonists (Fig. 1 *C–F*, Table S1). AhR agonists, dioxin (TCDD), cigarette smoke extract (CSE), benzo (*a*)pyrene (BAP), β-napthoflavone (βNF), and the partial agonist/antagonist α-napthoflavone (αNF) all activated ARPE19 cell AhRs (Fig. 1*C*). This activity was diminished with AhR antagonist treatment and upon AhR knockdown (Fig. 1 *C* and *D*). Expression of *CYP1A1* and *CYP1B1*, AhR-specific target genes, increased following AhR agonist treatment and once again diminished following AhR knockdown (Fig. 1 *E* and *F*). Hydroquinone (HQ), a benzopyrene and known component of cigarette smoke and environmental pollutants, also functioned as an AhR agonist, activating the receptor and increasing target gene expression (Fig. 1 *C–F*).

AhR Activity Decreases as a Function of Age. Because age is the primary demographic factor associated with AMD, we determined age-related differences in endogenous AhR transcriptional activity, normalized to ARPE19 transcriptional activity, in primary RPE cell lines derived from young (<55 y old) and old (>55 y old) human donors (Fig. 2 *A* and *B* and Table S2). A significant decrease in AhR activity and protein levels was observed with advanced age (Fig. 2 *A–D*, $P < 0.05$, $n = 5$ per age group) whereas *AhR* mRNA expression did not change significantly (Fig. 2*E*). The expression of *ARNT*, which complexes with ligand bound AhR and is a contributor to AhR activity, also did not change significantly with age (Fig. 2 *C* and *F*). Taken together, these findings suggest that the decreased AhR activity and protein levels may be associated with decreased DNA binding affinity of the AhR—ligand complex or altered recruitment of coactivators and corepressors necessary for downstream gene transcription (21). Given the observed decreased activity and protein expression of AhR with age in human RPE cells, we next examined the effect of AhR in the eye, in vivo, using *AhR*-null mice.

Retinal Function Is Impaired in $AhR^{-/-}$ Mice Reflecting RPE Cell Damage. To determine the role of AhR on visual function, we recorded electroretinograms (ERG) from 11-mo-old $AhR^{-/-}$ ($n = 8$, four female and four male) and age-matched wild-type mice ($n = 8$, four female and four male). Averaged ERG responses of dark-adapted $AhR^{-/-}$ mice under scotopic and photopic conditions revealed smaller b-wave amplitudes compared with age-matched wild-type mice at all flash intensities (Fig. 3 *A* and *C*). An approximately 50% reduction in scotopic b-wave amplitudes, and minor impairment of a-waves, quantitatively assessed by plotting average wave amplitudes as a function of flash intensity, were seen in $AhR^{-/-}$ mice (Fig. 3*B*). Because b-waves reflect the light responses of the ON-bipolar cells receiving inputs from photoreceptors, it is possible that the reduced b-wave amplitudes are a consequence of impaired photoreceptor light responses as revealed by the reduced a-waves. We investigated this possibility by calculating the ratio between b-wave amplitudes and a-waves evoked by the same flash intensity for wild-type and $AhR^{-/-}$ mice (Fig. 3*E*). We found that the ratios were essentially the same regardless of genotype, indicating that the reduced b-waves in $AhR^{-/-}$ mice are a consequence of im-

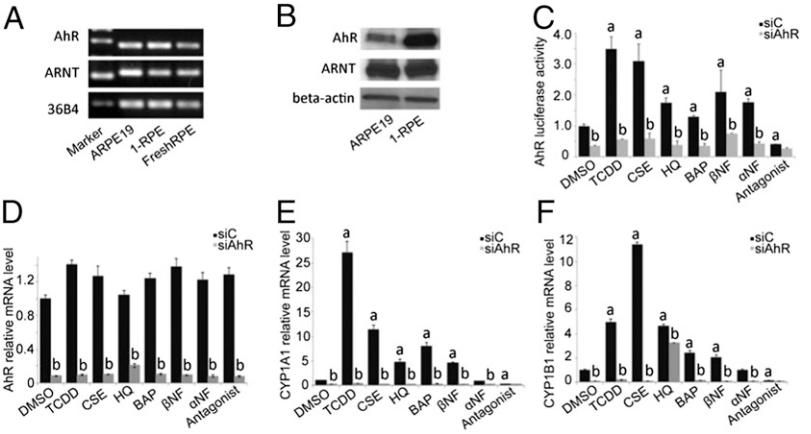

Fig. 1. AhR signaling pathway is active in human RPE cells. Each in vitro experiment was performed a minimum of three times. Data are means ± SEM for all graphs. a, Significantly different relative to DMSO treated cells ($P < 0.05$); b, significantly different relative to drug-SiC–-treated cells ($P < 0.05$). ARPE19 cell culture: 1-RPE, primary RPE cell culture, and FreshRPE, freshly harvested human RPE, express AhR and ARNT (*A*) mRNA and (*B*) protein. (*C*) AhR activity in ARPE19 cells following transfection with AhR-tk-luciferase reporter. Cells were treated with known agonists [10 nM TCDD, 1.50% cigarette smoke extract-CSE, 75 μM hydroquinone-HQ, 1 μM benzo(*a*)pyrene-BAP, 100 nM β-napthoflavone-βNF, 100 nM α-napthoflavone-αNF] and 1 μM AhR antagonist (Calbiochem182705) for the receptor for 24 h, with siRNA knockdown of the AhR or scrambled siRNA control (siC). (*D*) Using qPCR, decreased *AhR* mRNA was observed in ARPE19 cells following siRNA knockdown (gray bars) compared with scrambled siRNA control (black bars). mRNA expression of known AhR target genes (*E*) *CYP1A1* and (*F*) *CYP1B1* in ARPE19 cells treated with AhR agonists and an antagonist, for 24 h, with and without siRNA knockdown.

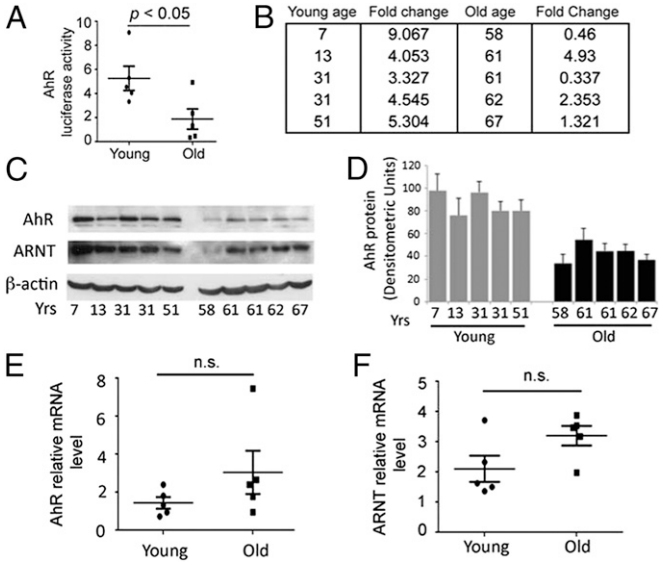

Fig. 2. Endogenous AhR activity in human RPE cells decreases as a function of age. Each in vitro experiment was performed a minimum of three times. Data are means ± SEM for all graphs, $P < 0.05$. Representative Western blots from four independent experiments are shown. (*A*) Box plot of endogenous AhR activity in RPE cell lines derived from young (<55 y; $n = 5$) and old (>55 y; $n = 5$) human donors ($n = 5$ per age group) normalized to AhR activity in ARPE19 cells. Each statistical significance was analyzed by Student's unpaired one-tailed *t* test; $P < 0.05$. (*B*) Details of AhR fold-activity changes and ages of each donor in young and old groups. (*C*) Western blot of AhR, ARNT, and housekeeping protein β-actin in young and old human donor RPE cell lines. (*D*) Densitometry measurements of the intensity of the AhR Western blot bands normalized to beta-actin for cell extracts. Box plot of (*E*) *AhR* and (*F*) *ARNT* mRNA relative to housekeeping gene 36B4 in young and old donor cell lines.

paired a-wave responses. We also observed reduced photopic cone-driven b-wave responses in the AhR knockouts similar to the effect on dark-adapted b-waves (Fig. 3 *C* and *D*), again with the b-wave/a-wave ratios being similar regardless of genotype (Fig. 3*E*), suggesting that the recorded ERG functional impairment of photoreceptors may be due to RPE cell damage (22).

To determine whether there is a morphological correlation with the visual function changes seen, we examined retinal sections from young and old $AhR^{-/-}$ mice. Although no noticeable differences were seen in the overall architecture of the outer retina of 3- and 6-mo-old $AhR^{-/-}$ (Fig. 3 *G* and *H*) compared with young and old wild-type mice (Fig. 3*F*), an age-dependent thinning of the inner and outer nuclear layers (INL and ONL, respectively) was observed at 11 and 16 mo in $AhR^{-/-}$ mice (Fig. 3 *I* and *J*, $P < 0.05$ for both INL and ONL of 11- and 16-mo-old $AhR^{-/-}$ mice, $n = 6$–10 images per mouse, $n = 11$–12 mice per genotype) (Figs. S1 and S2). However, no differences in the inner and outer segments were seen in 11-mo-old mice based on genotype, according to the immunohistochemical staining pattern of rhodopsin, the photopigment in the rod photoreceptor discs, and lectin staining using peanut agglutinin (PNA), which outlines the cone photoreceptor sheaths (Fig. S3). To determine whether the reduced b-wave amplitudes in $AhR^{-/-}$ mice correspond to morphological changes, we inspected the distribution, cell number and morphology of rod bipolar cells and cells in the inner plexiform and ganglion cell layers, in 11-mo-old $AhR^{-/-}$ and wild-type retinas using the immunohistochemical markers protein kinase c alpha (PKC α) and calretinin (Fig. S3). Again, no notable differences were observed in the staining pattern based on genotype. Our findings correlate with those of Chevallier et al., who recently examined young 3-mo-old *AhR*-null and wild-type mice and also did not find any difference in protein localization of secondary retinal neuronal markers (23). Markers for glial cells and synaptic vesicles, glial fibrillary acidic protein (GFAP), and synaptic vesicle 2 (SV2), respectively, were also used to evaluate possible genotype-associated variability in the retina; however, no differences were observed. These findings support our ERG results and suggest that the minor architectural changes observed in the ONL and INL thickness on examination of cross sections of the overlying retina in $AhR^{-/-}$ mice may be a consequence of RPE cell damage, as reported previously in human AMD (24).

AMD-Like RPE and Choroidal Pathology in $AhR^{-/-}$ Mice Develop as a Function of Age. The similar decrease in a- and b-wave ratios based on ERG analysis observed in our mice indicates an impairment of photoreceptor light activity that may be due to RPE damage (22). Therefore, we first examined autofluorescence accumulation, which is associated with RPE dysfunction in AMD (25), in retinal/RPE cyrosections from 11-mo-old $AhR^{-/-}$ and wild-type mice. We found a significant increase in lipofuscin-associated autofluorescence in $AhR^{-/-}$ animals (Fig. 4 *A–C*, $P < 0.05$, $n = 3$ sections per mouse, $n = 4$–5 mice per genotype). The Lambda (λ) scans showed a fluorescence spectrum with typical characteristics of lipofuscin (26). We observed a proportional increase in emission at all wavelengths and a 72% increase in RPE autofluorescence in $AhR^{-/-}$ compared with age-matched wild-type eyes. This increase in RPE autofluorescence was seen throughout the section and was not focally confined to a particular region of the eye. RPE morphology was further evaluated in flat mounts stained for filamentous actin (F-actin) using phalloidin labeling, which outlines the RPE cell (Fig. 4*D*). RPE cell-boundary disruptions and increased frequency of multinucleated RPE cells were seen in focal regions of flat mounts from $AhR^{-/-}$ mice. Notably, a similar pattern has been observed in RPE flat mounts from donor eyes with documented AMD (27).

Next, we further evaluated retinal/RPE/Bruch's membrane morphology in $AhR^{-/-}$ and wild-type mice. No differences were seen in 3- and 6-mo-old $AhR^{-/-}$ and aged-matched wild-type mice by light microscopy (Fig. 3 *F–H*) observations that were confirmed by electron microscopy. Evaluation of 11- and 16-mo-old wild-type mice with light and electron microscopy also appeared normal, with no significant changes observed in the retina or RPE/Bruch's membrane. In contrast, signs of RPE degeneration became evident at 11 mo of age in $AhR^{-/-}$ mice and included vacuolization and thick focal and diffuse sub-RPE deposits as well as regions of hyper-and hypopigmentation (Fig. 4*E* and Fig. S4*A*). More extensive vacuolization, pigmentary changes. and RPE atrophy were seen in 16-mo-old $AhR^{-/-}$ mice (Fig. 4*F* and Fig. S4*B*). Interestingly, on examination of posterior segment flat mounts, focal choroidal atrophy was seen in $AhR^{-/-}$ mice as early as 3 mo of age, the area of which increased with age (Fig. 5 *A* and *B*). Fundus and optical coherence tomography (OCT) imaging and transmission electron microscopy of 11-mo-old $AhR^{-/-}$ mice confirmed flat mount findings of choroidal thinning/atrophy (Fig. 5 *C* and *D*). Noteworthy, focal choroidal atrophy has recently been reported to occur in older individuals with posterior pole abnormalities and may also be associated with findings typical for AMD (28). In our $AhR^{-/-}$ mice, the regions of RPE abnormalities corresponded to areas with choroidal atrophy, but not exclusively, and, in fact, increased RPE autofluorescence and sub-RPE deposits in $AhR^{-/-}$ mice were seen throughout the eye. No evidence of choroidal or retinal neovascularization was observed in $AhR^{-/-}$ mice of any age.

Transmission electron microscopy was used for detailed examination of the RPE/Bruch's membrane complex (Fig. 6 and Table S3). Although 11-mo-old wild-type mice exhibited normal RPE morphology with organized basal infoldings and apical processes (Fig. 6*A*), age-matched $AhR^{-/-}$ mice had vacuolized RPE cell junctions (Fig. 6*B*), corresponding to the disrupted F-actin staining pattern observed in RPE flat mounts (Fig. 4*D*). Absence of basal infoldings (Fig. 6 *C* and *D*), thinning of RPE cells (Fig. 6*D*), and extensive continuous sub-RPE deposits

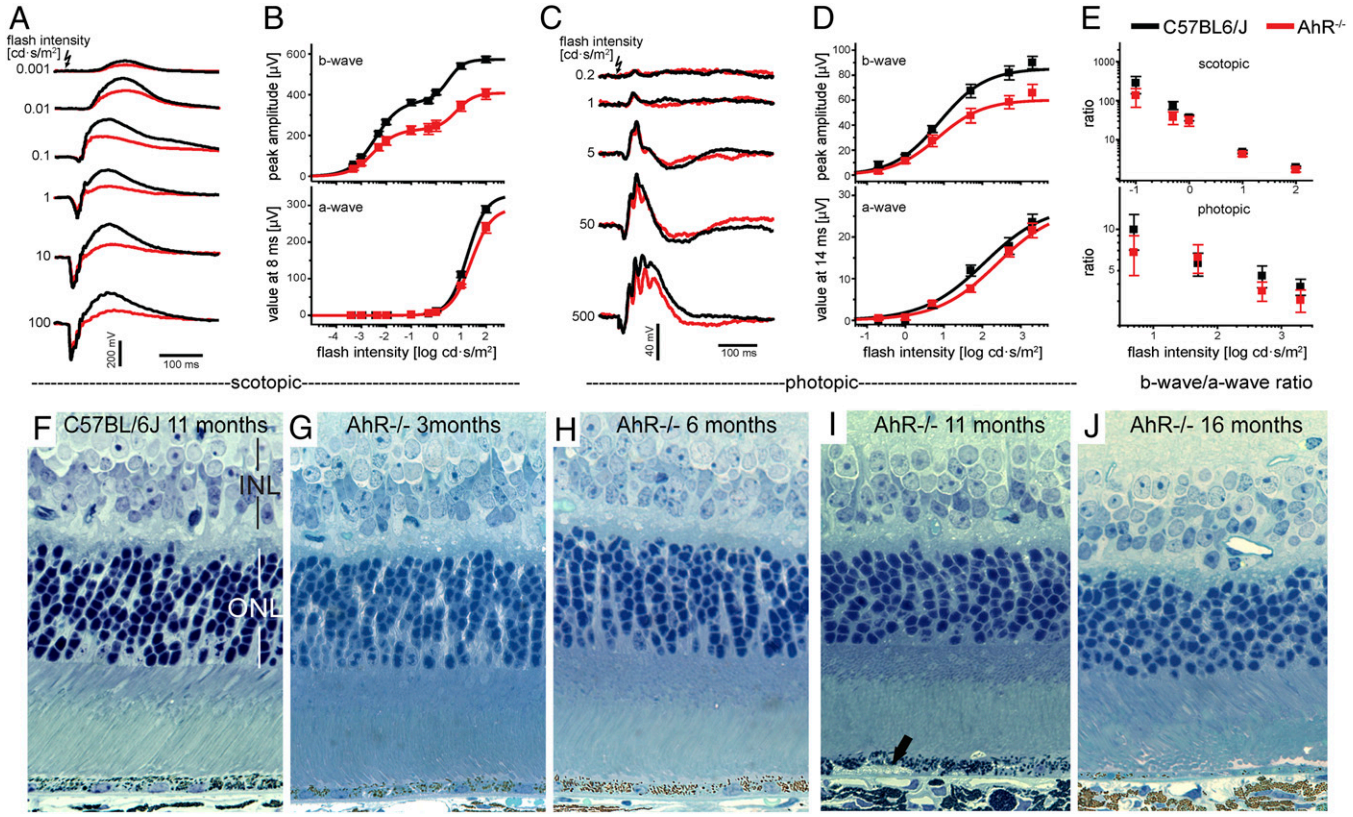

Fig. 3. *AhR*$^{-/-}$ mice have impaired visual function as a function of age. Electroretinograms in 11-mo-old *AhR*$^{-/-}$ and wild-type mice. (*A*) Averaged ERG responses from 11-mo-old dark-adapted *AhR*$^{-/-}$ mice (red; $n = 8$) and C57BL/6J wild-type controls (black; $n = 8$) evoked by flashes of increasing intensity under scotopic conditions. (*B*) Plots of dark-adapted b-wave amplitudes and a-waves as function of flash intensity. Data points (means ± SEM) were fitted to Eq. S1 (*SI Materials and Methods*), and fits are plotted as solid lines. (*C*) Averaged ERG responses from *AhR*$^{-/-}$ mice and wild-type controls exposed to rod-suppressing steady background illumination under photopic conditions. Responses were evoked by flashes of increasing intensity, as indicated. (*D*) Averaged b-wave amplitudes and a-waves (means ± SEM) were plotted as a function of flash intensity and fitted by one term of Eq. S1 (fits are shown as solid lines). (*E*) Ratios of b-wave amplitudes and a-waves were calculated for all flash intensities that evoked a-wave responses and were plotted as a function of flash intensities for scotopic (*Upper*) and photopic conditions (*Lower*), respectively. Morphology of retina/RPE in 1-μm-thick plastic sections stained with toluidine blue from an (*F*) 11-mo-old wild-type mouse, (*G*) 3-, (*H*) 6-, (*I*) 11-, and (*J*) 16-mo-old *AhR*$^{-/-}$ mice. Black arrow points to sub-RPE deposit. $n = 6$–10 images per mouse, $n = 11$–12 mice per genotype were examined.

below disrupted basal infoldings (Fig. 6 *E*–*G*) (seen in all eyes, >68% of area along the back of the eye cup), composed of amorphous electron dense material and fibrous long spacing collagen characteristic of basal laminar deposits, as seen in AMD (Fig. 6 *F* and *G*), were also seen in *AhR*$^{-/-}$ mice. Pigmentary changes observed included abundant melanogenesis and pigmentary degradation (Fig. 6 *H* and *I*). Overall incidence of AMD-related pathology observed in our cohort of mouse eyes is provided in Table S3.

Examination of the RPE/Bruch's membrane junction in wild-type mice at 16 mo of age appeared normal (Fig. 7*A*) whereas age-matched *AhR*$^{-/-}$ mice showed a progressive age-related increase in disorganized and absent RPE basal infoldings and RPE degeneration (Fig. 7*B*) (seen in all eyes, >38% of area along the back of the eye cup). Thick continuous deposits were evident underlying depigmented and atrophied RPE cells (Fig. 7 *C*–*E*). Considerable RPE pigmentary changes comprising hyperpigmentation (Fig. 7 *F* and *G*) and lipofuscin accumulation (Fig. 7*G*) were also observed. Noteworthy was the observation of basal linear deposit-like material including membranous debris and electron lucent droplets within Bruch's membrane of 16-mo-old *AhR*$^{-/-}$ mice (Fig. 7*H*). Basal linear deposits and drusen are regarded as hallmarks of early AMD and confer increased risk for progression (5). Finally, we measured the thickness of Bruch's membrane in wild-type and *AhR*$^{-/-}$ mice and found a significant increase in 11- and 16-mo-old *AhR*$^{-/-}$ mice (Fig. S1, $P < 0.01$ for both 11- and 16-mo-old cohorts, $n = 6$–10 images per mouse, $n = 11$–12 mice per genotype). Most of the increased thickness could be attributed to either a thickened, dense inner collagenous layer and/or expanded areas in the elastic layer (i.e., Fig. 7 *D* and *E*).

OxLDL and AhR Knockdown Stimulate Collagen IV Secretion from RPE Cells. Previously, McMillan and Bradfield (12) measured elevated levels of serum LDL in a cohort of young AhR-null mice. Additionally, they found that modified LDL using NaOCl oxidation is a potential agonist for AhR. With this in mind, we determined circulating levels of plasma LDL and HDL (high-density lipoprotein) in our cohort of aged 11-mo-old *AhR*$^{-/-}$ and wild-type mice. Although no differences were seen in body weights of mice based on genotype (Fig. 8*A*), we measured a significant increase in LDL, but not HDL, levels in *AhR*$^{-/-}$ compared with wild-type mice (Fig. 8 *B* and *C*, $P < 0.05$, $n = 12$–15 mice per genotype). Previously, oxLDL has been shown to stimulate extracellular matrix production. Because both LDL and oxLDL may contribute to the pathogenesis of AMD (29, 30), we examined the degree to which LDL and oxLDL regulate RPE production and secretion of collagen IV, an extracellular matrix molecule found in sub-RPE deposits, through AhR (Fig. 8 *D* and *E*). We found that, whereas AhR knockdown stimulates collagen IV secretion, treatment with oxLDL results in decreased collagen IV expression in cell extracts concomitant with an even

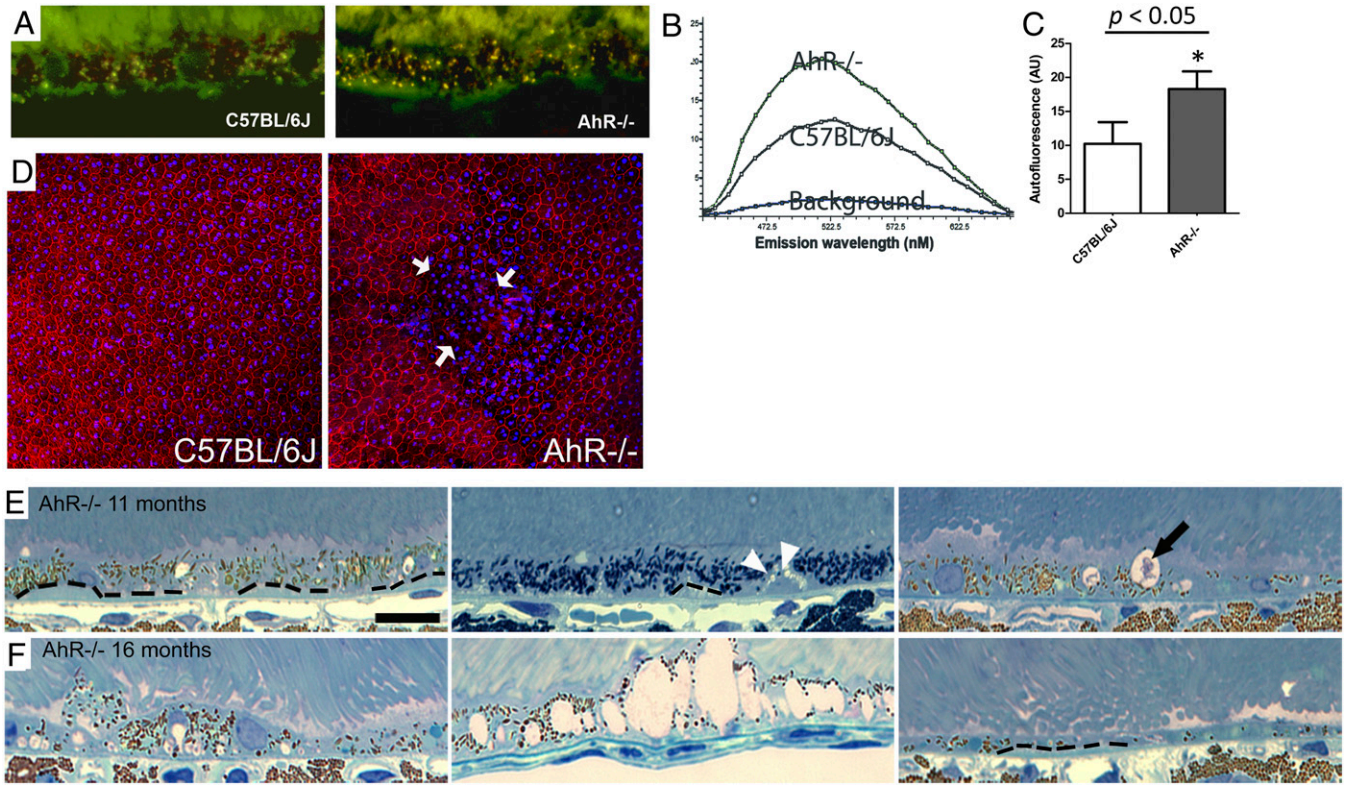

Fig. 4. Lipofuscin accumulation and structural changes in RPE of $AhR^{-/-}$ mice. For lipofuscin analysis, eyes from 11-mo-old C57BL/6J wild-type and $AhR^{-/-}$ mice were assessed by laser confocal microscopy. (*A*) Representative confocal fluorescence micrographs of the RPE layers showing lipofuscin granules in wild-type and $AhR^{-/-}$ knockout mice. (*B*) Spectral profile analyzed from λ scans displays the autofluorescence spectra profile from RPE of $AhR^{-/-}$ and wild-type animals. (*C*) Quantification of autofluorescence in the RPE layer in $AhR^{-/-}$ and wild-type mice. Data are means ± SEM, $n = 3$ sections per mouse, $n = 4$–5 mice per genotype, $P < 0.05$. (*D*) Flat mounts of the posterior eye from an 11-mo-old $AhR^{-/-}$ and wild-type mouse ($n = 4$ mice per genotype) stained with phalloidin (red), to outline the individual RPE cells. Disrupted RPE cell boarders are indicated by white arrows. Hoechst (blue) stains the nuclei in RPE/choroid/sclera (RPE facing up). Light microscopic images show photoreceptor outer segments/RPE/Bruch's membrane/choroid interface in (*E*) 11-mo-old $AhR^{-/-}$ mice, with diffuse sub-RPE deposits (outlined by dotted line), focal sub-RPE deposit (white arrowheads), and vacuolization (black arrow) and (*F*) 16-mo-old $AhR^{-/-}$ mice, with considerable RPE pigmentary changes, extensive vacuolization, RPE atrophy, and depigmentation. (Scale bar: 20 μm.) $n = 6$–10 images per mouse, $n = 11$–12 mice per genotype were examined with light microscopy.

larger relative increase in collagen IV secreted in the media (2.3-fold compared with AhR knockdown alone) (Fig. 8 *D* and *E*). A significant difference in collagen IV production was not seen in RPE cells treated with LDL. Interestingly, confirming previous studies that have shown oxLDL can increase extracellular matrix production in normal vascular smooth muscle cells (31), we also observed increased collagen IV secretion in siControl RPE cells (1.8-fold compared with DMSO-treated cells), supporting the hypothesis that oxLDL may be stimulating extracellular matrix production through induction of more than one pathway (32). In vivo, increased collagen IV staining and protein were confirmed in the RPE/choroid of $AhR^{-/-}$ mice by immunofluorescence and Western blot analysis (Fig. 8 *F*–*H*), complementing our observation of fibrous long spacing collagen in sub-RPE deposits in these mice (Fig. 6 *F* and *G*). Localization of collagen in basal laminar deposits and thickened Bruch's membrane has previously been reported in human AMD histological sections (4). Finally, one-week ("chronic") knockdown of AhR in ARPE19 cells also resulted in elevated expression of extracellular matrix molecules, including collagen IV, fibronectin, and the extracellular matrix regulator, transforming growth factor-β (TGF-β) (Fig. 8*I*). Together, these data suggest that the absence of AhR may stimulate collagen secretion from RPE cells, promoting extracellular accumulation within deposits, Bruch's membrane, and choroid.

Discussion

We report on a previously undescribed role of the endogenous AhR in sub-RPE debris accumulation and subsequent development of dry AMD. We demonstrate an age-related decrease in AhR activity and expression, the consequence of which may be a disruption in the healthy cellular metabolic response to endogenous and exogenous compounds. We found that $AhR^{-/-}$ mice have impaired visual function, comparable to that reported in AMD patients (33, 34). $AhR^{-/-}$ mice also presented with key features of dry AMD, including an age-related thinning of the INL and ONL, accumulation of fibrous long-spacing collagen-containing sub-RPE deposits, leading to RPE loss analogous to geographic atrophy. The accumulation of extracellular matrix molecules in deposits of these mice appears to be controlled both directly and potentially indirectly through AhR. Direct regulation is supported by the results of the 1-wk AhR knockdown study in RPE cell culture, demonstrating increased extracellular matrix molecule expression whereas the indirect regulation may occur through increased serum lipoproteins, which in turn stimulates extracellular matrix molecule production and secretion from RPE cells. It has been proposed that, early in life, mechanisms are in place within RPE cells that allow for removal of basally shed RPE debris, thus the absence of sub-RPE deposits in young individuals (35), and that age-related disruptions to these clearance mechanisms may lead to deposits. Our findings support a role for the AhR signaling pathway in sub-RPE debris clearance, a mechanism that becomes less active with age, and may therefore contribute to disease pathogenesis.

AMD is a multifactorial disorder, without identifiable direct causative factors. The complexity of AMD and number of potential initiating mechanisms proposed to date suggest that susceptibility

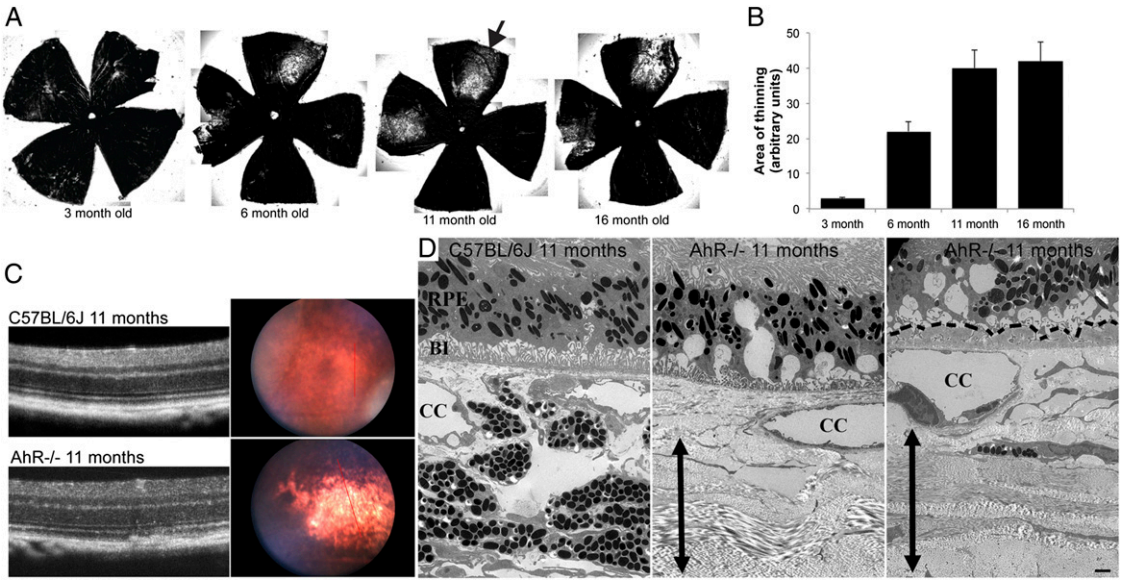

Fig. 5. Choroidal atrophy in $AhR^{-/-}$ mice with age. (*A*) Flat mounts of RPE/choroid from 3- to 16-mo-old $AhR^{-/-}$ mice showing progressive choroidal thinning (lighter area-black arrow). (*B*) Graph of mean area of thinning versus age measured from flat mounts. (*C*) Fundus images of 11-mo-old $AhR^{-/-}$ and wild-type mice with choroidal thinning (right). The red lines correspond to plane of optical coherence tomography (OCT) image (*Left*). n = 3 mice per genotype examined. (*D*) Electron micrographs of choroidal atrophy in 11-mo-old $AhR^{-/-}$ compared with C57BL/6J mice. BI, basal infoldings; CC, choriocapillaris; RPE, retinal pigment epithelium. Double-headed black arrow spans the length of the sclera. Basal laminar deposits are outlined by black dashed lines. n = 6–10 images per mouse, n = 11–12 mice per genotype were examined. (Scale bar: 2 μm.)

to disease is attributable in part to human variability. Our study results support this idea, in that we observed lower AhR activity in RPE cells derived from many of our older donors compared with activity in younger donors, although not all older human samples showed diminished activity. This variability is consistent with the fact that not all older individuals develop AMD and that, among those who do, there are differences in time of onset and progression rate. Still, our study provides strong evidence for the concept that individuals with lower versus higher AhR activity may not be as well equipped to metabolize structurally diverse endogenous and exogenous AhR ligands, including xenobiotic, chemical, lipid, and drug insults. Mechanistically, this potential metabolic challenge may be relevant to older smokers and individuals with hypercholesterolemia, who, based on epidemiological studies, are reported to have a higher risk for developing AMD (3).

A prevailing AMD pathogenic paradigm is extracellular matrix dysregulation (36), which may lead to disruption of normal transport of nutrients and removal of waste products across Bruch's membrane. We found that one mechanism by which AhR may influence deposit formation is through extracellular matrix regulation. We show that, in the absence of AhR, there is increased collagen, fibronectin, and TGFβ expression in, and/or secreted from, RPE cells. Collagen and fibronectin are components of sub-RPE deposits and Bruch's membrane, and TGFβ is a regulator of extracellular matrix production (37). Furthermore, in vivo, the absence of AhR results in elevated circulating levels of LDL, which in the oxidized form can increase collagen secretion from RPE cells in an AhR-dependent manner. Interestingly, oxLDL in RPE cells expressing basal levels of AhR also secrete collagen as previously reported in smooth vascular muscle and mesangial cells (31, 32), indicating that the effect of oxLDL specifically on extracellular matrix production may be occurring through multiple pathways (32). Additional AMD-related pathogenic pathways that may be regulated by AhR and need to be investigated in detail include hypoxia, inflammation, alterations in lipid metabolism (38), and the ubiquitin–proteosomal pathway. Finally, oxidative stress has also been linked to AMD pathogenesis in several animal models, through pathways involving superoxide dismutase 1 (SOD1) (39), SOD2 (40), and nuclear respiratory factor 2 (NRF2) (41). Nonetheless, to date, there are no studies that have demonstrated decreased SOD or NRF activity in RPE cells derived from human donor tissue. Interestingly, AhR regulates both SOD1 and -2 (42) and cross-talks with NRF2 (43).

Cardiovascular disease, increased body mass index, elevated serum LDL, and cholesterol levels are risk factors for AMD progression (44, 45) and provide support for lipid dysregulation as a pathogenic pathway of AMD. Because AhR has also been shown to play a role in cholesterol homeostasis and metabolic pathways (46), an interesting finding in our study is the effect of $AhR^{-/-}$ on serum LDL levels in aged mice, similar to previous reports of elevated circulating LDL in young $AhR^{-/-}$ mice (12). To further elucidate the role of AhR on lipid metabolism, we fed a cohort of 11-mo-old $AhR^{-/-}$ and wild-type mice (n = 15) a high fat/high cholesterol diet (HFD) for 8 wk (Fig. S5). HFD consumption by $AhR^{-/-}$ mice resulted in a high mortality rate (73.4%, n = 11/15) and a low survival rate of 26.6% (n = 4/15) by 8 wk postinitiation of diet, compared with wild-type mice on the diet (survival rate of 93%, n = 14/15). These results support previous microarray studies demonstrating AhR as a critical regulator of lipid and cholesterol biosynthesis and lipogenesis (18, 19). Noteworthy, the observed elevated LDL levels in our $AhR^{-/-}$ may also be in part due to the fact that young $AhR^{-/-}$ mice have been reported to develop expanded corneal limbal vessels of the eye and patent ductus venosus because of either increased blood pressure or failure in vasoconstriction in the liver (47), which in turn may influence lipid metabolism. Regardless, our demonstration of elevated LDL levels in the absence of AhR expression in vivo, along with decreased AhR activity and protein expression in human RPE cells with age, and reports showing increased serum cholesterol and LDL levels in AMD patients (48) support a potential interplay between AhR and cholesterol/lipid homestasis in disease progression (18, 19, 49). Future studies using tissue-specific knockout of AhR will serve to further tease out the relationship between AhR, lipid metabolism, and disease progression.

In this study, we have shown accumulation of basal linear-like deposits in 16-mo-old $AhR^{-/-}$ mice. Although previous studies

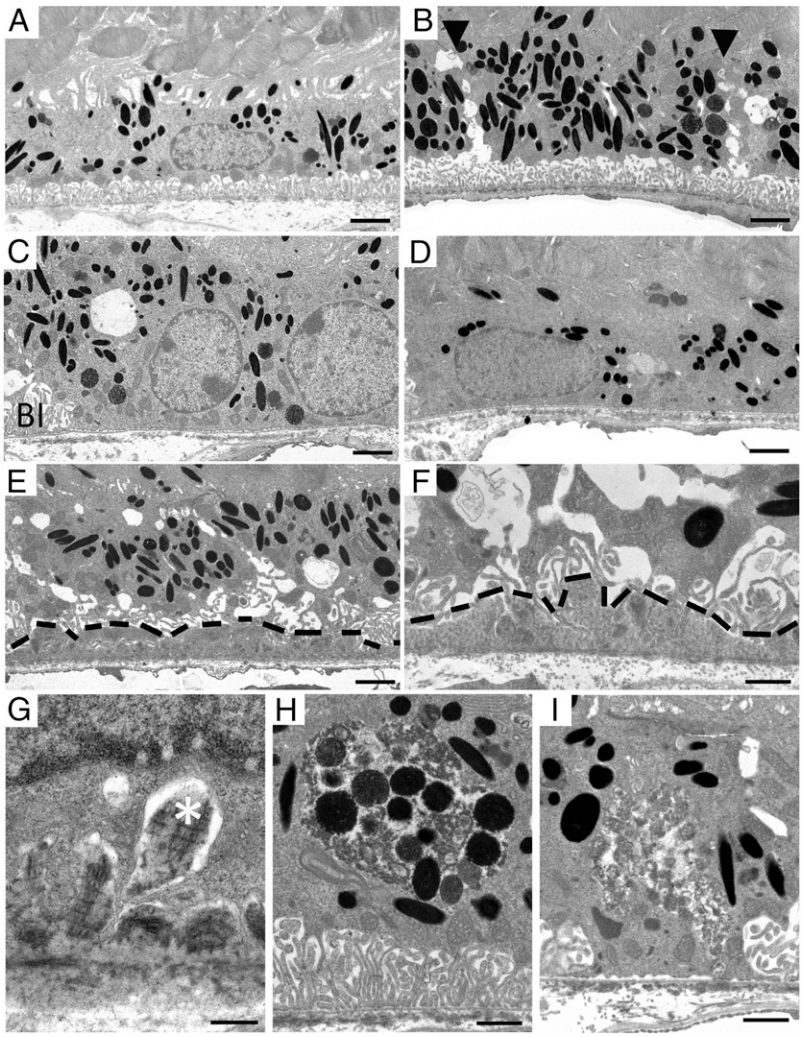

Fig. 6. Ultrastructural changes in 11-mo-old $AhR^{-/-}$ mice. Electron micrographs of RPE/Bruch's membrane/choroidal junction in (*A*) 11-mo-old wild-type mice appear normal whereas 11-mo-old $AhR^{-/-}$ mice show (*B*) hyperpigmentation and vacuolization along the RPE junction (black arrowheads), (*C*) loss of basal infoldings, (*D*) thinning of the RPE cell layer and hypopigmentation, (*E*) continuous basal laminar deposits containing (*F* and *G*) fibrous long spacing collagen (white asterisk), and pigmentary changes including (*H*) melanogenesis and (*I*) melanin degradation. BI, basal infoldings. Basal laminar deposits are outlined by black dashed lines. n = 6–10 images per mouse, n = 11–12 mice per genotype were examined. (Scale bars: *A*–*E*, 1 μm; *F*–*I*, 2 μm.)

have described linear-like deposits in various transgenic mice, on closer examination, it is apparent that these mice exhibit thickened elastic and collagenous layers in Bruch's membrane (41, 50) rather than membranous debris accumulation (5). Morphologically, basal linear deposits are associated with increased risk of AMD (5). Another unique finding in the $AhR^{-/-}$ mice was the observation of focal regions of choroidal thinning or atrophy. These regions corresponded with a high concentration of basal

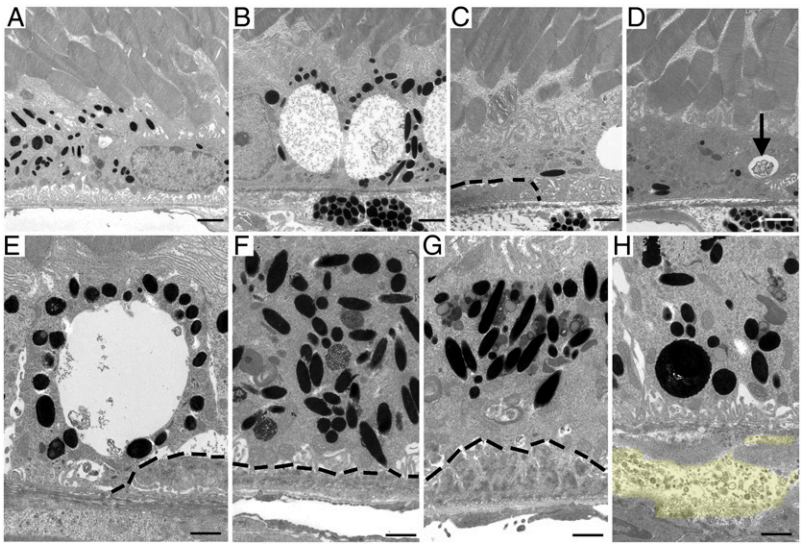

Fig. 7. Ultrastructural changes in 16-mo-old $AhR^{-/-}$ mice. Electron micrographs of RPE/Bruch's membrane/choroidal junction in (*A*) 16-mo-old wild-type mice appear normal whereas age-matched $AhR^{-/-}$ mice show (*B*) extensive vacuolization, (*C*) RPE atrophy overlying basal laminar deposit, (*D*) RPE atrophy, depigmentation, and vacuole containing membranous material (black arrow), (*E*) large vacuole adjacent basal laminar deposits, (*F*) hyperpigmentation, and accumulated lipofuscin in RPE cells overlying thin, and (*G*) thick continuous basal laminar deposits and (*H*) accumulation of basal linear like-deposit material (yellow highlight) within Bruch's membrane. Basal laminar deposits are outlined by black dashed lines. n = 6–10 images per mouse, n = 11–12 mice per genotype were examined. (Scale bars: *A*–*D*, 1 μm; E–H, 2 μm.)

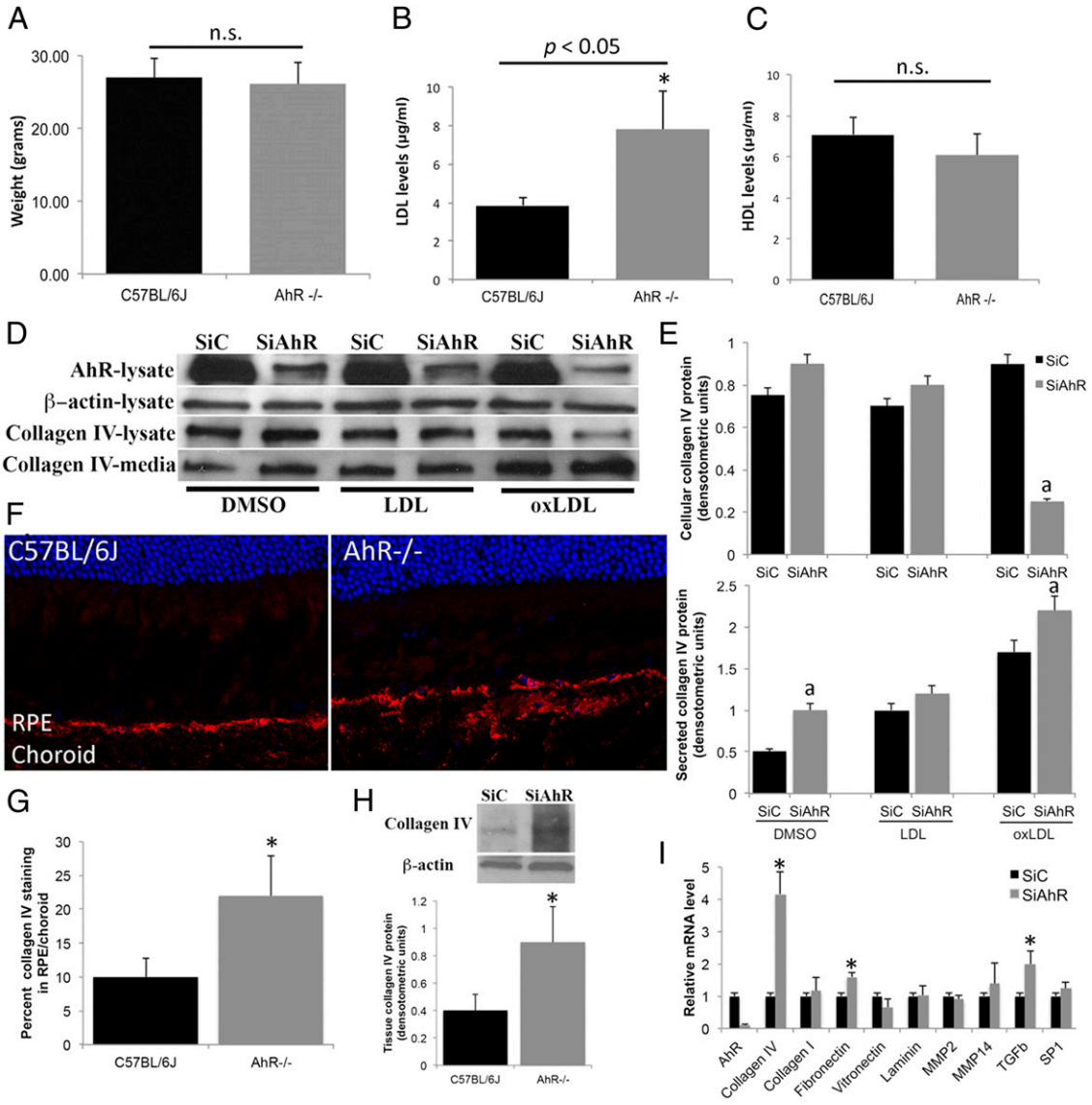

Fig. 8. OxLDL and AhR knockdown stimulate extracellular matrix production by RPE cells. (*A*) Average weight of 11-mo-old C57BL/6J wild-type and $AhR^{-/-}$ mice. Serum (*B*) low-density lipoprotein (LDL) and (*C*) high-density lipoprotein (HDL) levels in 11-mo-old wild-type and $AhR^{-/-}$ mice. Data are means ± SEM for weight and lipid levels. n = 12–15 mice per genotype. Statistical significance was analyzed by Student t test; $P < 0.05$. (*D*) Western blot analysis of collagen IV expression in ARPE19 cells transfected with scrambled siRNA control (siC) and siRNA targeting AhR (siAhR) and treated with 50 μg/mL LDL and 50 μg/mL oxLDL for 48 h, measured in whole-cell extract and secreted media. Representative data from three independent experiments are shown. (*E*) Densitometry measurements of the intensity of the Western blot bands normalized to beta-actin for cell extracts and secreted media normalized to total protein loaded values. (*F*) Confocal immunofluorescence images depicting collagen IV (red) distribution in 11-mo-old wild-type and $AhR^{-/-}$ mice. Cell nuclei are stained with Hoechst 33342 (blue). (*G*) Percent collagen IV immunofluorescence staining in RPE/choroid relative to entire area of RPE/choroid in cryosections from $AhR^{-/-}$ and C57BL/6J mouse eyes. A minimum of three sections from the nasal, temporal and central regions of the eyes were evaluated in n = 8 mice per genotype. (*H*) Western blot of collagen IV protein levels in RPE/choroid tissue samples harvested from $AhR^{-/-}$ and C57BL/6J mouse eyes. Densitometry measurements of intensity of the Western blot bands normalized to beta-actin. Representative data from two independent experiments are shown. (*I*) Extracellular matrix mRNA expression in ARPE19 cells by qPCR, following 1-wk chronic AhR knockdown and normalized to the housekeeping gene 36B4. The asterisk represents $P < 0.05$. Each in vitro cell culture experiment was performed a minimum of three times. Data are means ± SEM for all graphs. a, Significantly different relative to drug-SiC treated cells ($P < 0.05$).

deposits, supporting recent observations of increased density of drusen above areas of choriocapillary dropout (51). However, deposits were also seen in other quadrants of $AhR^{-/-}$ mouse eyes not associated with overt choroidal vasculature change. This finding and full characterization of the choroidal vasculature should be a focus of study.

It remains to be investigated why the absence of AhR affects RPE cells more than other retinal cells, such as photoreceptors and choroidal endothelial cells. To address AhR activity in photoreceptors, availability of high-fidelity in vitro models is necessary as AhR activity cannot be accurately assessed in human tissue samples. We have, however, evaluated relative AhR activity in RPE (ARPE19) compared with choroidal endothelial (RF/6A) cells and found endogenous AhR activity in ARPE19 cells to be 8.5-fold higher than in RF/6A cells (Fig. S6). Results of visual function analysis in our cohort of $AhR^{-/-}$ versus wild-type mice also support a greater gene effect on RPE cells rather than the photoreceptor cells. Although, morphologically, we were able to detect some thinning of the ONL and INL in 11-mo-old $AhR^{-/-}$ relative to wild-type mice, the observed thinning

could be due to the presence of diffuse sub-RPE deposits in the eyes. A similar finding of thinning of the ONL and INL overlying drusen has been reported in AMD patients (24). Furthermore, a difference in localization of protein markers for secondary retinal neurons was not seen in $AhR^{-/-}$ versus wild-type mice. This finding is similar to that of Chevallier et al., who recently identified nystagmus in young 10-wk-old AhR null mice (23). In their $AhR^{-/-}$ mice, as old as 3 mo, they also did not see any differences in localization of bipolar, amacrine, and horizontal cell markers based on genotype. It is, however, noteworthy that the *AhR*-null mice used by Chevallier et al. were produced on a C57BL/6N background (52) and carry a retinal degeneration mutation (RD8). Those mice are different from our cohort of AhR mice, which are on the C57BL/6J background (52) and do not harbor the retinal phenotypic complication of an RD8 mutation (Fig. S7).

This study reports on the AhR signaling pathway in RPE cells and its potential role in the pathogenesis of AMD (Fig S8). Our results indicate that there is an age-related decrease in AhR activity and expression in human RPE cells that could lead to a decrease in cellular xenobiotic metabolism and matrix metabolism, resulting in accumulation of extracellular matrix molecules and debris (sub-RPE deposits), as seen in early dry AMD, and, with progressive age, RPE degeneration or geographic atrophy, as seen in late dry AMD. Overall, our analysis of retinal function and phenotype of $AhR^{-/-}$ mice revealed substantial AMD-like lesions, establishing these mice as a model for further investigating mechanisms underlying initiation and progression of disease. Therefore, studies should focus on exploring the contribution of other AhR functions to disease pathology and the therapeutic potential of targeting AhR as a means to prevent or remove deposit accumulation.

Materials and Methods

Cell Culture. Passages 25–30 of ARPE19 cells, a cell line from a 19-y-old male donor, obtained from the American Type Culture Collection, were used in this study. Primary RPE cell cultures and freshly isolated RPE cells were obtained from donor eyes collected from the North Carolina Organ Donor and Eye Bank, Inc., less than 6 h postmortem and cultured within 24 h, in accordance with the Declaration of Helsinki for research involving human tissue. Human samples used in this study included young (<55 y) and old (>55 y) donors listed in Table S2 and were harvested from nondiabetic donors without a history of ocular disease. Eyes appeared grossly normal under microscopic examination. RPE cells were isolated as previously described for cell culture (53) or collected in RNAlater preservative (Invitrogen/Life Technologies) for RNA studies (54).

siRNA Transfection. The control small interfering RNA (siRNA) for a nontargeting sequence and siRNA for AhR (QIAGEN) were reverse transfected into cells using Lipofectamine RNAiMAX (Invitrogen) according to the manufacturer's protocol (54). Mock transfection and scrambled siRNA served as additional controls. ARPE19 or primary RPE cells were added to each well with phenol-red-free DMEM/F12 or MEM media plus 7.5% (vol/vol) charcoal stripped FBS. After 24 h, cells were treated with drugs for 24 or 48 h. For chronic 1-wk transfection, 3 d after the first treatment, a second knockdown was performed. RNA and protein were extracted for real-time PCR (Table S4) and Western blot assay (Table S5).

Transcriptional Activation Assays. Transcriptional activity of AhR was assessed using a luciferase-based reporter and target gene qPCR assays (54). Lipofectin (Invitrogen)-mediated transfection was performed in cultured cells using plasmid DNAs of AhR-Tk-Luciferase, CMV-β-galactosidase, and pBSII (55). After 24 h, cells were treated with agonists and antagonists at doses listed in Table S1. Luciferase (reporter) and β-galactosidase [chlorophenol red-β-D-galactopyranoside (CPRG) as substrate; transfection normalization] activities were measured using a Perkin-Elmer Fusion Instrument. For activation assays with siRNA transfection, cells were transfected with siRNA, following plasmid DNA transfection. Five hours postknockdown, cells were treated with drugs and lysed 24 h later for luminescence reading. Concomitantly cells were treated with these same compounds for RNA and gene-expression studies. All samples were run in triplicate, and experiments were performed a minimum of three times.

Mice. AhR-deficient mice ($AhR^{-/-}$ strain B6.129-AhR^{tm1Bra}J) obtained from The Jackson Laboratory were bred and aged at The Hamner Institutes for Health Sciences and Duke University. The AhR strain carries a targeted deletion of exon 2 of the AhR gene and was backcrossed for 12 generations onto C57BL/6J (52). $AhR^{-/-}$ mice were genotyped for the rd8 mutation to rule out genetic retinal degeneration (Fig. S7 and *SI Materials and Methods*). Age-matched C57BL/6J mice purchased from The Jackson Laboratory served as wild-type controls. All animal procedures were performed under the supervision of the Duke University Institutional Animal Care and Use Committee. Effect of diet on genotype was evaluated in 11-mo-old $AhR^{-/-}$ and wild-type mice fed a high fat diet (Cocoa butter diet, T.D. 88051; Harlan Teklad) or normal diet as previously described (56). Mice were weighed, and blood serum samples were collected at time of euthanasia. Eyes were collected for light and electron microscopy.

Electroretinography. ERGs were recorded using the Espion E^2 system (Diagnosys LLC) as described previously (57). Briefly, 11-mo-old wild-type and $AhR^{-/-}$ mice were dark-adapted overnight and anesthetized by an i.p. injection of a ketamine/xylazine mixture (85/10 mg/kg). Pupils were dilated with 1% cyclopentolate-HCl and 2.5% phenylephrine, and the mouse body temperature was maintained at 37 °C using a water-based warming pad. ERG responses under dark-adapted ("scotopic") conditions were evoked by a series of nine flashes ranging from 0.0001 cd·s/m^2 to 100 cd·s/m^2. For flashes up to 0.1 cd·s/m^2, responses of 10 trials were averaged. For 0.5 and 1 cd·s/m^2 flash responses, three trials were averaged. For brighter stimuli, responses to single flashes were recorded without averaging. Light-adapted ("photopic") ERGs were evoked by a series of six flashes ranging from 0.2 cd·s/m^2 to 2,000 cd·s/m^2 whereas rod inputs were suppressed with a steady background illumination of 50 cd/m^2. Up to 10 trials were averaged for all flash responses. Analysis of a- and b-wave amplitudes was performed as described (57). For details of data analysis, see *SI Materials and Methods*.

RPE Flat-Mount Preparation. Post enucleation, the anterior segment of eyes from 11-mo-old wild-type and $AhR^{-/-}$ mice was removed, and the neural retina was dissected from unfixed posterior eyecups. For phalloidin staining of the RPE (Table S5), eyes were fixed in -RPE flat mounts under light microscopy. The area of thinning was measured relative to total area of flat mount and digitally analyzed using ImageJ software.

Brightfield and Optical Coherence Tomography Imaging. A Micron III (Phoenix Research Laboratories Inc.) retinal imaging microscope was used to obtain brightfield images from selected anesthetized 11-mo-old wild-type and $AhR^{-/-}$ mice. The OCT module of the Micron III was used to image retinal layers guided from the brightfield.

Lipofuscin Quantification. A Leica Spectral Laser Scanning Confocal Microscope was used to measure autofluorescence throughout the entire RPE layer of 11-mo-old $AhR^{-/-}$ and wild-type cryosections (n = 3 sections per mouse, n = 4–5 mice per genotype) as previously described (58). The three sections were selected randomly from the nasal, central, and temporal regions of the mouse eye. Lambda (λ) scans were performed using a 405-nm laser. Excitation and emission frequencies were measured with a 5-nm-wide band through a spectral range from 422.5 nm to 722.5 nm using serial 30-image scans at ∼10.3-nm intervals. Fluorescent intensities are represented as arbitrary units as defined by the confocal Leica software. The significance of differences in spectra obtained between $AhR^{-/-}$ and wild-type mice was assessed using a two-tailed t test, with no variance assumptions.

Lipid Profile Measurement. HDL and LDL/VLDL-cholesterol assay kit was used to measure serum HDL and VLDL/LDL-cholesterol concentrations (Abcam) in 11-mo-old wild-type and $AhR^{-/-}$ mice (n = 12–15 per cohort). Fifty microliters of serum from each mouse was diluted with 50 μL of dIH_2O. This solution was then mixed with 100 μL of precipitation buffer to separate out the HDL and LDL/vLDL. Assays were performed in accordance with the manufacturer's instructions, and final data were extrapolated from a standard curve.

Statistical Analysis and Data Collection. One- and two-tailed Student t tests were performed with Excel, MATLAB, or GraphPad Prism. Values were considered statistically significant for $P < 0.05$ and have been indicated in figures. Each in vitro experiment was repeated a minimum of three times. Western blots shown are representative of a minimum of three independent experiments.

Detailed methodology is described in *SI Materials and Methods*.

ACKNOWLEDGMENTS. We thank the North Carolina Eye Bank, the eye donors, and their families for their generosity. We give sincere thanks to Drs. Steven Fliesler, Boris Reidel, and Joel Meyer for scientific discussions and helpful comments, Dr. Ying Hao for assistance with electron microscopy, Dr. Mayur Choudhary for technical assistance, Mr. Jim Ahrendsen and Mr. Scott Johnston from Phoenix Research Laboratories for support with brightfield and OCT imaging of mice, and Dr. Chad Grotegut for assistance with the cigarette smoke extract protocol. This work was supported by the US National Institutes of Health Grants EY02868 (to G.M.), P30 EY005722 (to Duke Eye Center), EY019688 and EY021626 (to M.E.B.), and DK48807 (to D.P.M.), by Research to Prevent Blindness, Inc. (RPB) core grants to the Duke Eye Center, by the American Health Assistance Research Foundation-Macular Degeneration (G.M.), by an RPB Special Scholars Award (to G.M.), and by an Alcon Young Investigator Award (to G.M.).

1. Klein R, Lee KE, Gangnon RE, Klein BE (2013) Incidence of visual impairment over a 20-year period: The Beaver Dam Eye Study. *Ophthalmology* 120(6):1210–1219.
2. Baird PN, et al. (2008) Gene-environment interaction in progression of AMD: The CFH gene, smoking and exposure to chronic infection. *Hum Mol Genet* 17(9):1299–1305.
3. Tomany SC, et al. (2004) Risk factors for incident age-related macular degeneration: Pooled findings from 3 continents. *Ophthalmology* 111(7):1280–1287.
4. Sarks S, Cherepanoff S, Killingsworth M, Sarks J (2007) Relationship of Basal laminar deposit and membranous debris to the clinical presentation of early age-related macular degeneration. *Invest Ophthalmol Vis Sci* 48(3):968–977.
5. Curcio CA, Millican CL (1999) Basal linear deposit and large drusen are specific for early age-related maculopathy. *Arch Ophthalmol* 117(3):329–339.
6. Anderson DH, et al. (2010) The pivotal role of the complement system in aging and age-related macular degeneration: Hypothesis re-visited. *Prog Retin Eye Res* 29(2): 95–112.
7. Crabb JW, et al. (2002) Drusen proteome analysis: An approach to the etiology of age-related macular degeneration. *Proc Natl Acad Sci USA* 99(23):14682–14687.
8. Wang L, et al. (2010) Abundant lipid and protein components of drusen. *PLoS ONE* 5(4):e10329.
9. McIntosh BE, Hogenesch JB, Bradfield CA (2010) Mammalian Per-Arnt-Sim proteins in environmental adaptation. *Annu Rev Physiol* 72:625–645.
10. Phillips DH (1999) Polycyclic aromatic hydrocarbons in the diet. *Mutat Res* 443(1-2): 139–147.
11. Adachi J, et al. (2001) Indirubin and indigo are potent aryl hydrocarbon receptor ligands present in human urine. *J Biol Chem* 276(34):31475–31478.
12. McMillan BJ, Bradfield CA (2007) The aryl hydrocarbon receptor is activated by modified low-density lipoprotein. *Proc Natl Acad Sci USA* 104(4):1412–1417.
13. Savouret JF, et al. (2001) 7-ketocholesterol is an endogenous modulator for the arylhydrocarbon receptor. *J Biol Chem* 276(5):3054–3059.
14. Kung T, Murphy KA, White LA (2009) The aryl hydrocarbon receptor (AhR) pathway as a regulatory pathway for cell adhesion and matrix metabolism. *Biochem Pharmacol* 77(4):536–546.
15. De Abrew KN, Kaminski NE, Thomas RS (2010) An integrated genomic analysis of aryl hydrocarbon receptor-mediated inhibition of B-cell differentiation. *Toxicol Sci* 118(2): 454–469.
16. Hillegass JM, Murphy KA, Villano CM, White LA (2006) The impact of aryl hydrocarbon receptor signaling on matrix metabolism: Implications for development and disease. *Biol Chem* 387(9):1159–1173.
17. Ohtake F, et al. (2007) Dioxin receptor is a ligand-dependent E3 ubiquitin ligase. *Nature* 446(7135):562–566.
18. Sato S, et al. (2008) Low-dose dioxins alter gene expression related to cholesterol biosynthesis, lipogenesis, and glucose metabolism through the aryl hydrocarbon receptor-mediated pathway in mouse liver. *Toxicol Appl Pharmacol* 229(1):10–19.
19. Tanos R, Murray IA, Smith PB, Patterson A, Perdew GH (2012) Role of the Ah receptor in homeostatic control of fatty acid synthesis in the liver. *Toxicol Sci* 129(2):372–379.
20. Esfandiary H, Chakravarthy U, Patterson C, Young I, Hughes AE (2005) Association study of detoxification genes in age related macular degeneration. *Br J Ophthalmol* 89(4):470–474.
21. McDonnell DP, Norris JD (2002) Connections and regulation of the human estrogen receptor. *Science* 296(5573):1642–1644.
22. Noell WK (1980) Possible mechanisms of photoreceptor damage by light in mammalian eyes. *Vision Res* 20(12):1163–1171.
23. Chevallier A, et al. (2013) Oculomotor deficits in aryl hydrocarbon receptor null mouse. *PLoS ONE* 8(1):e53520.
24. Sadigh S, et al. (2013) Abnormal thickening as well as thinning of the photoreceptor layer in intermediate age-related macular degeneration. *Invest Ophthalmol Vis Sci* 54(3):1603–1612.
25. Sparrow JR, Boulton M (2005) RPE lipofuscin and its role in retinal pathobiology. *Exp Eye Res* 80(5):595–606.
26. Thampi P, et al. (2012) The 5HT1a receptor agonist 8-Oh DPAT induces protection from lipofuscin accumulation and oxidative stress in the retinal pigment epithelium. *PLoS ONE* 7(4):e34468.
27. Ding JD, et al. (2011) Anti-amyloid therapy protects against retinal pigmented epithelium damage and vision loss in a model of age-related macular degeneration. *Proc Natl Acad Sci USA* 108(28):E279–E287.
28. Spaide RF (2009) Age-related choroidal atrophy. *Am J Ophthalmol* 147(5):801–810.
29. Picard E, et al. (2010) CD36 plays an important role in the clearance of oxLDL and associated age-dependent sub-retinal deposits. *Aging (Albany, NY Online)* 2(12): 981–989.
30. Yin L, et al. (2011) OX-LDL up-regulates the vascular endothelial growth factor-to-pigment epithelium-derived factor ratio in human retinal pigment epithelial cells. *Curr Eye Res* 36(4):379–385.
31. Jimi S, Saku K, Uesugi N, Sakata N, Takebayashi S (1995) Oxidized low density lipoprotein stimulates collagen production in cultured arterial smooth muscle cells. *Atherosclerosis* 116(1):15–26.
32. Abdelsamie SA, et al. (2011) Oxidized LDL immune complexes stimulate collagen IV production in mesangial cells via Fc gamma receptors I and III. *Clin Immunol* 139(3): 258–266.
33. Gerth C (2009) The role of the ERG in the diagnosis and treatment of Age-Related Macular Degeneration. *Doc Ophthalmol* 118(1):63–68.
34. Li J, Tso MO, Lam TT (2001) Reduced amplitude and delayed latency in foveal response of multifocal electroretinogram in early age related macular degeneration. *Br J Ophthalmol* 85(3):287–290.
35. Johnson LV, et al. (2011) Cell culture model that mimics drusen formation and triggers complement activation associated with age-related macular degeneration. *Proc Natl Acad Sci USA* 108(45):18277–18282.
36. Zarbin MA (2004) Current concepts in the pathogenesis of age-related macular degeneration. *Arch Ophthalmol* 122(4):598–614.
37. Leask A, Abraham DJ (2004) TGF-beta signaling and the fibrotic response. *FASEB J* 18(7):816–827.
38. Kishan AU, Modjtahedi BS, Martins EN, Modjtahedi SP, Morse LS (2011) Lipids and age-related macular degeneration. *Surv Ophthalmol* 56(3):195–213.
39. Imamura Y, et al. (2006) Drusen, choroidal neovascularization, and retinal pigment epithelium dysfunction in SOD1-deficient mice: a model of age-related macular degeneration. *Proc Natl Acad Sci USA* 103(30):11282–11287.
40. Justilien V, et al. (2007) SOD2 knockdown mouse model of early AMD. *Invest Ophthalmol Vis Sci* 48(10):4407–4420.
41. Zhao Z, et al. (2011) Age-related retinopathy in NRF2-deficient mice. *PLoS ONE* 6(4): e19456.
42. Rico de Souza A, et al. (2011) Genetic ablation of the aryl hydrocarbon receptor causes cigarette smoke-induced mitochondrial dysfunction and apoptosis. *J Biol Chem* 286(50):43214–43228.
43. Shin S, et al. (2007) NRF2 modulates aryl hydrocarbon receptor signaling: Influence on adipogenesis. *Mol Cell Biol* 27(20):7188–7197.
44. Ebrahimi KB, Handa JT (2011) Lipids, lipoproteins, and age-related macular degeneration. *J Lipids* 2011:802059.
45. Seddon JM, Cote J, Davis N, Rosner B (2003) Progression of age-related macular degeneration: Association with body mass index, waist circumference, and waist-hip ratio. *Arch Ophthalmol* 121(6):785–792.
46. Lee JH, et al. (2010) A novel role for the dioxin receptor in fatty acid metabolism and hepatic steatosis. *Gastroenterology* 139(2):653–663.
47. Lahvis GP, et al. (2005) The aryl hydrocarbon receptor is required for developmental closure of the ductus venosus in the neonatal mouse. *Mol Pharmacol* 67(3):714–720.
48. Reynolds R, Rosner B, Seddon JM (2010) Serum lipid biomarkers and hepatic lipase gene associations with age-related macular degeneration. *Ophthalmology* 117(10): 1989–1995.
49. Angrish MM, Dominici CY, Zacharewski TR (2013) TCDD-elicited effects on liver, serum, and adipose lipid composition in C57BL/6 mice. *Toxicol Sci* 131(1):108–115.
50. Jones A, et al. (2011) Increased expression of multifunctional serine protease, HTRA1, in retinal pigment epithelium induces polypoidal choroidal vasculopathy in mice. *Proc Natl Acad Sci USA* 108(35):14578–14583.
51. Mullins RF, Johnson MN, Faidley EA, Skeie JM, Huang J (2011) Choriocapillaris vascular dropout related to density of drusen in human eyes with early age-related macular degeneration. *Invest Ophthalmol Vis Sci* 52(3):1606–1612.
52. Lahvis GP, Bradfield CA (1998) Ahr null alleles: Distinctive or different? *Biochem Pharmacol* 56(7):781–787.
53. Jaffe GJ, Earnest K, Fulcher S, Lui GM, Houston LL (1990) Antitransferrin receptor immunotoxin inhibits proliferating human retinal pigment epithelial cells. *Arch Ophthalmol* 108(8):1163–1168.
54. Dwyer MA, Kazmin D, Hu P, McDonnell DP, Malek G (2011) Research resource: nuclear receptor atlas of human retinal pigment epithelial cells: Potential relevance to age-related macular degeneration. *Mol Endocrinol* 25(2):360–372.
55. DuSell CD, et al. (2010) Regulation of aryl hydrocarbon receptor function by selective estrogen receptor modulators. *Mol Endocrinol* 24(1):33–46.
56. Malek G, et al. (2005) Apolipoprotein E allele-dependent pathogenesis: A model for age-related retinal degeneration. *Proc Natl Acad Sci USA* 102(33):11900–11905.
57. Herrmann R, Lee B, Arshavsky VY (2011) RGS9 knockout causes a short delay in light responses of ON-bipolar cells. *PLoS ONE* 6(11):e27573.
58. Cai J, et al. (2012) β-Secretase (BACE1) inhibition causes retinal pathology by vascular dysregulation and accumulation of age pigment. *EMBO Mol Med* 4(9):980–991.